MODULATION SPECTROSCOPY OF RYDBERG EXCITONS

SVEN BODENSTEDT

University of Stuttgart
Germany

Bachelor Thesis

Supervisor: Prof. Dr. Harald Gießen

4th Physics Institute
Faculty 8: Mathematics and Physics
University of Stuttgart

November 2015

Sven Bodenstedt: *Modulation Spectroscopy of Rydberg Excitons,* © November 2015

ABSTRACT

This thesis deals with the generation and investigation of highly excited Rydberg excitons in the semiconductor cuprous oxide (Cu_2O). The two fundamental parts of the setup are an external cavity diode laser (ECDL) and a waveguide of periodically poled magnesium oxide-doped lithium niobate (MgO:PPLN).

The cuprous oxide crystal used was artificially grown at the Max Planck Institute for Solid State Research (Stuttgart). It is shown for the first time that artificially grown Cu_2O crystals can show exciton absorptions up to at least the main quantum number $n = 9$. Usually natural Cu_2O crystals are used for experiments, due to the superior crystal quality. This thesis shows that the theoretical model for the description of excitons fits with a high accuracy to the experimental data.

Moreover different methods of modulation spectroscopy are tested. For this setup only the amplitude modulation spectroscopy leads to good results. It is shown that the signal-to-noise ratio (SNR) could be increased compared to normal transmission spectroscopy.

ZUSAMMENFASSUNG

Diese Abschlussarbeit behandelt die Erzeugung und Untersuchung von hoch angeregten Rydberg Exzitonen im Halbleiter Kupferoxydul (Cu_2O). Der Versuchsaufbau besteht hauptsächlich aus einer Laserdiode mit einem externem Resonator (ECDL), sowie einem Wellenleiter aus periodisch gepoltem Lithiumniobat, welcher mit Magnesiumoxid dotiert ist (MgO:PPLN).

Der verwendete Kupferoxydul Kristall ist künstlich am Max Planck Institut für Festkörperforschung (Stuttgart) gewachsen. Es wird zum ersten Mal gezeigt, dass auch künstliche Cu_2O Kristalle Exzitonenanregungen bis zur Hauptquantenzahl $n = 9$ zeigen können. Normalerweise werden aufgrund der besseren Kristallqualität natürliche Kristalle für Experimente mit Kupferoxydul verwendet. Diese Arbeit zeigt, dass das theoretische Modell für die Beschreibung von Exzitonen sehr gut mit den experimentellen Ergebnissen übereinstimmt.

Außerdem werden verschiedene Methoden der Modulationsspektroskopie getestet. Mit diesem Versuchsaufbau führte nur die Amplitudenmodulationsspektroskopie zu guten Ergebnissen. Das Signal-Rausch-Verhältnis (SNR) konnte im Vergleich zu gewöhnlicher Transmissionspektroskopie erhöht werden.

ACKNOWLEDGMENTS

I'm deeply grateful to my supervisor Prof. Dr. Harald Gießen, who affords me to work on this interesting and exciting project and supports me, whenever there occurred a problem. I would like to thank also my advisor Tobias Steinle for his great assistance during the whole experiment and thesis. I want to thank Moritz Fischer, who helped me building the setup and doing the measurements.

It is a pleasure to thank the 1st Physics Institute and its director Prof. Dr. Martin Dressel, who provides the facilities for this experiments. My special thanks goes to Eric Heintze, Dr. Yuan Yan and Uwe Pracht, who instructed us in the handling of the cryostat and sample mounting. This thesis would not have been possible unless the support and instruction of the facility of cryogenics (Tieftemperaturtechnik).

I would like to thank the Max Planck Institute for Solid State Research. My thank goes especially to Chengtian Lin, who provides the high quality artificial cuprous oxide crystal and also Annette Zechtmeister and Barbara Baum for cutting and polishing the samples.

I owe my deepest gratitude to my friends and family, espacially my parents, who are helping me not only by reading and correcting my thesis.

CONTENTS

INTRODUCTION 1

i THEORY 3

1 SEMICONDUCTORS 5
- 1.1 General Properties 5
  - 1.1.1 Band Structure 5
  - 1.1.2 Effective Masses 6
  - 1.1.3 Excitons 7
  - 1.1.4 Phonons 8
- 1.2 Cuprous Oxide 9
  - 1.2.1 Crystal Structure 9
  - 1.2.2 Rydberg Excitons 10

2 OPTICS 11
- 2.1 Linear Optics 11
  - 2.1.1 Electromagnetic Wave 11
  - 2.1.2 Fabry-Pérot Interferometer 12
  - 2.1.3 Grating 13
- 2.2 Nonlinear Optics 14
  - 2.2.1 Second Harmonic Generation 14
  - 2.2.2 Quasi-Phase Matching 15
- 2.3 Lasers 16
  - 2.3.1 Laser Diode 16
  - 2.3.2 Littrow ECDL 17

3 SPECTROSCOPY 19
- 3.1 Linewidth 19
- 3.2 Modulation Spectroscopy 20
  - 3.2.1 Lock-In Amplifier 20
  - 3.2.2 Amplitude Modulation Spectroscopy 21
  - 3.2.3 Frequency Modulation Spectroscopy 22

ii EXPERIMENT 25

4 SETUP 27
- 4.1 Tunable Diode Laser 27
- 4.2 Waveguide 27
- 4.3 Filter, Noise Eater and Spectrum Analyzer 27
- 4.4 Chopper, Photo Diode and Lock-In Amplifier 28
- 4.5 Cryostat 28
- 4.6 Samples 29

5 METHOD OF MEASUREMENT 31
- 5.1 Amplitude Modulation Spectroscopy 31
- 5.2 Frequency Modulation Spectroscopy 31

iii RESULTS 33
6 LASER 35
6.1 Power 35
6.1.1 Influence of Current 35
6.1.2 Influence of Temperature 35
6.2 Spectrum 37
6.2.1 Influence of Temperature 37
6.2.2 Influence of Piezo Voltage 38
6.3 Mode-Hop Free Tuning 38
6.3.1 Indicators 38
6.3.2 Properties 40
6.3.3 Influence of Frequency 41
7 WAVEGUIDE 43
8 CUPROUS OXIDE 45
8.1 Calibration 45
8.2 Fit Of Absorption Lines 45
8.3 Analysis 47
8.3.1 Linewidth and Oscillator Strength 47
8.3.2 Binding Energy 48
8.4 Limitations 49

CONCLUSION 51

OUTLOOK 53

iv APPENDIX 55
A EXCITON ENERGIES OF THE YELLOW SERIES 57

BIBLIOGRAPHY 59

LIST OF FIGURES

Figure 1 Band structure of the semiconductor gallium arsenide. 6
Figure 2 Different types of phonon-assisted photon absorption. 8
Figure 3 Structure of Cu_2O. 9
Figure 4 Rydberg Excitons of Cu_2O up to $n = 25$. 10
Figure 5 Fabry-Pérot interferometer. 12
Figure 6 Reflection diffraction grating. 13
Figure 7 Difference between no and quasi-phase matching. 15
Figure 8 Littrow configuration. 17
Figure 9 Mode selection of a Littrow ECDL. 18
Figure 10 Absorbtion spectrum of a particle with two energy states. 19
Figure 11 Operating principle of a simple lock-in amplifier. 20
Figure 12 Simple amplitude modulation setup. 21
Figure 13 Simple frequency modulation setup. 22
Figure 14 Principle of frequency modulation spectroscopy. 22
Figure 15 Scheme of the experimental setup. 28
Figure 16 Sample holder with two samples. 29
Figure 17 Influence of current on the power. 36
Figure 18 The influence of the temperature on the laser power. 36
Figure 19 Spectrum of the laser. 37
Figure 20 The influence of the temperature on the central wavelength. 38
Figure 21 Voltage's influence on the central wavelength (with mode-hops). 39
Figure 22 Difference of the mode-hop free tuning. 39
Figure 23 Influence of the voltage on the central wavelength (mode-hop free). 40
Figure 24 Ideal temperature for the quasi-phase match condition. 44
Figure 25 Spectrum of the SHG. 44
Figure 26 Spectrum of the yellow exciton series of an artificial Cu_2O crystal at 1.9 K up to the main quantum number $n = 9$. 46
Figure 27 Fit of a single absorption line ($n = 5$). 46

Figure 28 Analysis of exciton absorption linewidth parameters. 48

LIST OF TABLES

Table 1 Fit parameters E_n, Γ_n and C_n of the absorption lines. 47
Table 2 Fit parameters q_n, a_n and b_n of the absorption lines. 47
Table 3 Average radius and lifetime of the measured excitons 49
Table 4 High-precision exciton energies of the yellow series in Cu_2O. 57

ACRONYMS

APP Anamorphic Prism Pairs

AR Anti-Reflection

CW Continuous Wave

DC Direct Current

ECDL External-Cavity Diode Laser

FM Frequency Modulation

FSR Free Spectral Range

FWHM Full Width at Half Maximum

MgO:PPLN Periodically Poled Magnesium Oxide doped Lithium Niobate

MPI Max Planck Institute

PBS Polarizing Beamsplitter

SHG Second Harmonic Generation

SNR Signal-to-Noise Ratio

INTRODUCTION

The process where a material absorbs light of a certain energy to get into an excited state is basis of many fields of research. The easiest and best understood system regarding this is the hydrogen atom, which consists only of a single proton and a single electron. The energy levels are well known and can be calculated precisely.

A highly excited arbitrary atom can be described analogously to the hydrogen atom. The so called Rydberg atom combines the simplicity of the hydrogen atom with the variety of the periodic table's elements.

Excitons are bounded states in a semiconductor, which can also be described analogously to the hydrogen atom. If they are also highly excited they can be called Rydberg excitons with similar properties as the atom's representatives. Due to their large spatial extension and long lifetime they are potential candidates for technical applications such as quantum devices.

This thesis is about the construction of an experimental setup and the evaluation of methods of measurement to investigate Rydberg excitons. The experiments are implemented with the semiconductor material Cu_2O. As the method of measurement the technique of modulation spectroscopy is applied.

The thesis is divided into three parts: The first part explains the theoretical background of semiconductors, optics and spectroscopy. The second part is about the experimental setup and describes the method of measurement. The last part shows the results of the measurements we did. It contains details of both the setup and the excitons of the semiconductor system.

The thesis clarifies, whether the chosen setup and methods of measurement are suitable for the investigation of Rydberg excitons in Cu_2O and so offers the possibility for many further research projects.

Part I

THEORY

1 SEMICONDUCTORS

1.1 GENERAL PROPERTIES

A *semiconductor* is a solid state crystal with an electrical conductivity between that of a conductor and an insulator. As a solid state material, most of its physical properties arise from the periodic structure of its atoms.

1.1.1 *Band Structure*

An electron in a solid state material can be described by a *Bloch function*

$$\psi_{nk}(\mathbf{r}) = e^{i\mathbf{k}\cdot\mathbf{r}} u_{nk}(\mathbf{r}), \tag{1}$$

where $u_{nk}(\mathbf{r})$ is a periodic function, which has the same periodicity as the solid state crystal. The real vector $\mathbf{k}$ is called the *wave vector* and its possible values depend on the boundary conditions of the system. The vector $\mathbf{r}$ describes the position within the crystal. The variable n is called the main quantum number and will be explained later.

The Bloch function is the most general solution of the *time-independent Schrödinger equation*

$$E_{nk}\psi_{nk}(\mathbf{r}) = \left(\frac{\mathbf{P}^2}{2m} + V(\mathbf{r})\right)\psi_{nk}(\mathbf{r}) \tag{2}$$

of a system which has a periodic potential $V(\mathbf{r})$ and only one particle of the mass m. The symbol $\mathbf{P}$ stands for the impulse operator and $\hbar$ is the reduced *Planck constant*. Although this is only an approximation of the real situation inside the crystal, it describes many properties very well and sufficiently.

The energies of the solutions vary continuously with the variation of $\mathbf{k}$ and thus form an energy band of continuous energy states. For a single wave vector $\mathbf{k}$ there are furthermore multiple solutions of the Schrödinger equation, which are labeled by the variable n. Combining these leads to an electronic *band structure* which determines many properties of a solid state crystal. It is possible, that there is no solution for some energies between the bands. These forbidden energy levels are called *band gaps* and are important for the classification of solid state materials.

The bands are filled with electrons up to the *Fermi energy*, which is a material specific constant. If the Fermi energy is within a band gap of a few eVs the solid state crystal is called a semiconductor. The

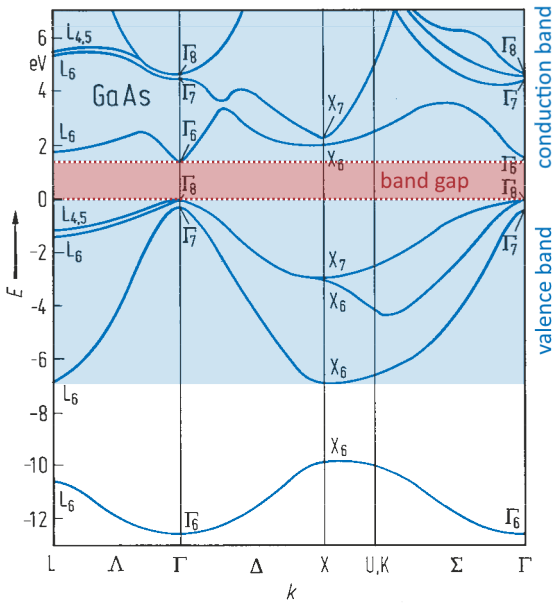

Figure 1: Band structure of the semiconductor gallium arsenide. [1]

highest completely filled band is called the *valence band*, while the next higher empty or partly filled band is called *conduction band*. Figure 1 shows as an example the band structure of the semiconductor gallium arsenide, which has a clearly visible band gap of about 1 eV between the valence band and the conduction band.

1.1.2 *Effective Masses*

The mathematical space of all possible wave vectors $\mathbf{k}$ is called the *reciprocal space*. The origin of the reciprocal space ($\mathbf{k} = 0$) is named the Γ-Point. Close to the Γ-Point the bands are almost isotropic and can be approximated by a parabola of the form

$$E(\mathbf{k}) = \frac{\hbar^2 \mathbf{k}^2}{2m_e^*} \quad . \tag{3}$$

By comparing this with the dispersion relation of a free electron

$$E(\mathbf{k}) = \frac{\mathbf{p}^2}{2m_e} = \frac{\hbar^2 \mathbf{k}^2}{2m_e} \tag{4}$$

and using the identity $\mathbf{p} = \hbar\mathbf{k}$ for the impulse $\mathbf{p}$, it seems natural to label the constant m_e^* as an *effective mass* of an electron in a solid state crystal.

If one electron of the semiconductor's valence band is moved to the conduction band, it has almost the same physical properties as a free electron, except the reduced mass. The other electrons left in the valence band can be described by a single particle with a positive charge, which is called a *hole*. Like the single electron in the conduction band a hole has similar physical properties to a free particle. In

other words it has an effective mass m_h^* and can be described by the same dispersion relation.

1.1.3 *Excitons*

When an electron moves from the valence to the conduction band a hole is created. These electron-hole pairs can usually move locally independently and are not bound to each other. Based on the Coulomb interaction between the electron and the hole it is also possible to create bound electron-hole-pairs, which are called *excitons*. The energy that is required to create an exciton is due to the binding energy below the energy of the band gap.

There are two distinguishable sorts of excitons: The *Frenkel* excitons can be observed mainly in solid states of molecules, noble gases or ions and have a binding energy of about 1 eV. *Mott-Wannier* excitons have a very small binding energy of about 10 meV and are typical for excitons in semiconductors. [2]

The most general equation for the possible energies of *Mott-Wannier* excitons

$$E_n = E_g - \frac{\mu^* e^4}{32\pi^2\hbar^2\epsilon_r^2\epsilon_0^2}\frac{1}{n^2} + \frac{\hbar^2\mathbf{K}^2}{2(m_e^* + m_h^*)} \tag{5}$$

is similar to the equation of a *hydrogen atom* [2]. In the last equation μ^* is the reduced mass of the exciton, which is defined using the equation $\mu^{*-1} = m_e^{*-1} + m_h^{*-1}$. The other constants are the elementary charge e, the relative permittivity ϵ_r, the vacuum permittivity ϵ_0, the energy of the band gap E_g and the wave vector of the exciton $\mathbf{K}$, which describes the center of mass motion. The relative motion of a hole and an electron is described similar to the hydrogen atom, by the angular momentum quantum number $l = 0, 1, 2, \ldots$ and the main quantum number n.

Similar to the hydrogen atom, a *Bohr radius*

$$a_B = \frac{4\pi\hbar^2\epsilon_r\epsilon_0}{\mu^* e^2} \tag{6}$$

and a *Rydberg energy*

$$E_R = \frac{\mu^* e^4}{32\pi^2\hbar^2\epsilon_r^2\epsilon_0^2} = \frac{e^2}{8a_B\pi\epsilon_r\epsilon_0} \tag{7}$$

can be defined.

If a photon is absorbed by a semiconductor to create an exciton, the conservation of energy and impulse has to be preserved. The maximum absolute impulse of an electron can be estimated by the equation

$$|\mathbf{p}_{\text{electron}}| = \hbar\,|\mathbf{k}| = \frac{h}{a}\ , \tag{8}$$

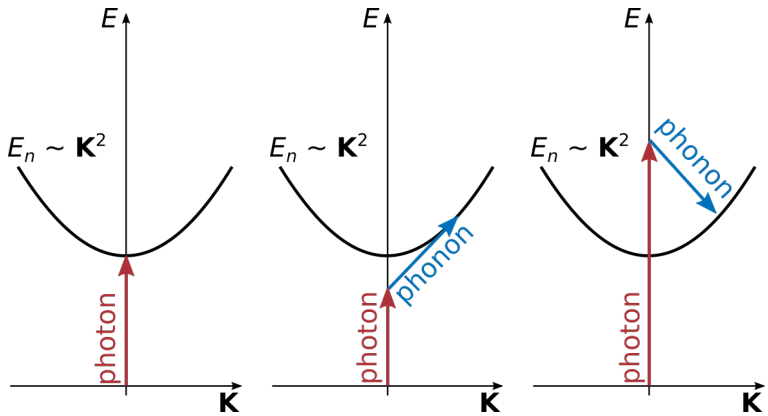

(a) Photon only. (b) Phonon absorbed. (c) Phonon emitted.

Figure 2: Different types of phonon-assisted photon absorption.

where a is the lattice constant.

The absolute impulse of a photon

$$\left|\mathbf{p}_{\text{photon}}\right| = \hbar\,|\mathbf{k}| = \frac{h}{\lambda} \tag{9}$$

is because of $\lambda \gg a$ small compared to the electron impulses. Therefore the absolute impulse and also the wave vector $\mathbf{K}$ of an exciton created by a simple photon absorption is negligible and can be set to zero.

1.1.4 *Phonons*

Phonons are quasiparticles within a solid state crystal, which have an impulse $\mathbf{p} = \hbar\mathbf{q}$ and an energy $E = h\nu_{\mathbf{q}}$. They are the quantum mechanical concept to describe the oscillation of the atoms in the lattice. If a phonon interacts with other particles like photons, the conservation of energy

$$h\nu_{\text{emission}} = h\nu_{\text{absorption}} + h\nu_{\mathbf{q}} \tag{10}$$

and impulse

$$\hbar\mathbf{k}_{\text{emission}} = \hbar\mathbf{k}_{\text{absorption}} + \hbar\mathbf{q} + \hbar\mathbf{Q} \tag{11}$$

holds with the exception of the additional impulse $\hbar\mathbf{Q}$, where $\mathbf{Q}$ can be any reciprocal lattice vector.

With the so called *phonon-assisted photon absorption* it is possible to create excitons with a non-zero resulting impulse $\mathbf{K}$. In this situation a phonon is absorbed or emitted during the photon absorption and it transfers its impulse to the exciton. This process is outlined in Figure 2.

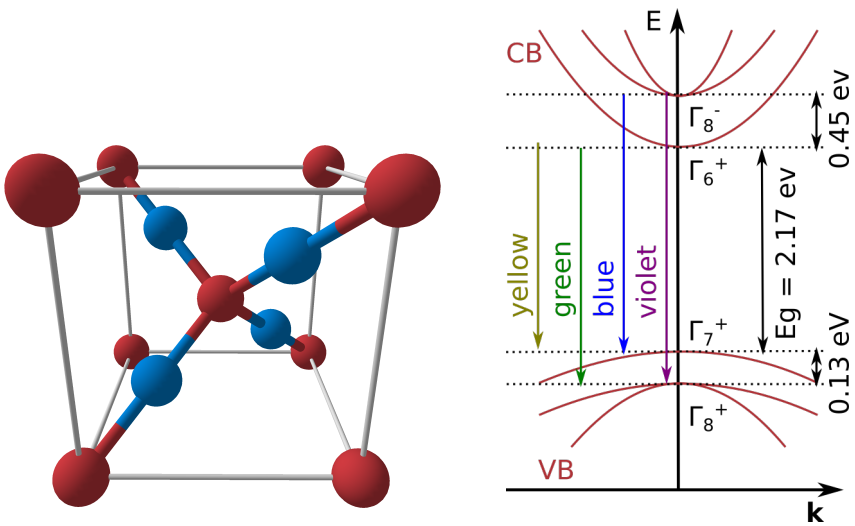

(a) Crystal structure of Cu_2O.

(b) Schematic band structure of Cu_2O.

Figure 3: Structure of Cu_2O [3]. a) Crystal structure of Cu_2O. The O-atoms (red spheres) are positioned in a bcc-lattice. The Cu-atoms (blue spheres) are arranged in an fcc-lattice, which is, compared to the other lattice, shifted by a quarter of the diagonal length. b) Schematic band structure of Cu_2O around the center of the first Brillouin zone. There is a direct band gab of 2.17 eV, which forms the yellow exciton series.

1.2 CUPROUS OXIDE

Cuprous oxide is a red inorganic solid with the formula Cu_2O. Other names are Copper(I) oxide, cuprite, red copper oxide or dicopper oxide.

1.2.1 *Crystal Structure*

The physical properties of a semiconductor depend strongly on the crystal quality. Usually natural Cu_2O-crystals are superior in this respect compared to artificial ones. In this experiment both types will be investigated.

Figure 3 shows the crystal and band structure of cuprous oxide (Cu_2O). The O-atoms are arranged in a bcc-latice and the Cu-atoms in an fcc-lattice. The lattices are shifted to each other by a quarter of the diagonal length. [3]

As shown in Figure 3b Cu_2O has a direct band gap of about 2.17 eV, which corresponds to a wavelength in the visible spectrum of about 571 nm.

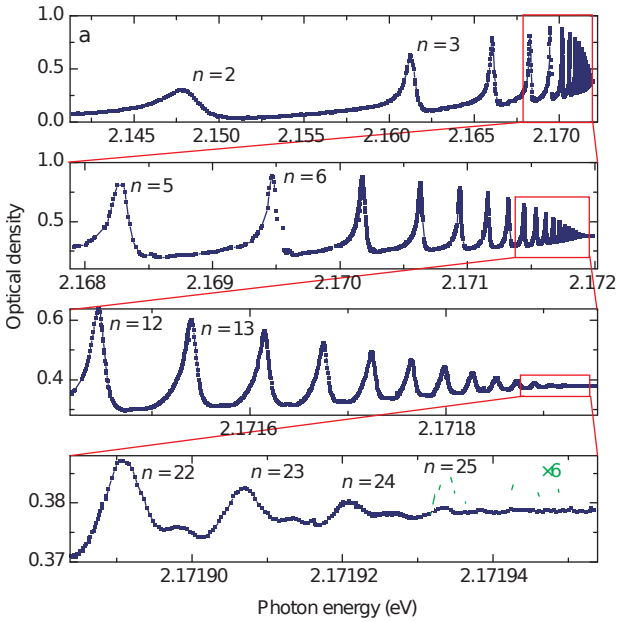

Figure 4: Rydberg Excitons of Cu_2O up to $n = 25$. [3]

1.2.2 *Rydberg Excitons*

As shown in Figure 3b there are four possible electron transitions, which can form the four (yellow, green, blue and violet) exciton series. Due to the parity S-excitons ($l = 1$) are dipole forbidden, while P-excitons ($l = 2$) are dipole allowed.

The energy levels of the yellow exciton series

$$E_n = E_g - \frac{E_R}{(n - \delta_P)^2} \tag{12}$$

are similar to Equation 5, with the exception that the concept of a quantum defect δ_P is applied, as discussed in [3].

By now Figure 4 shows the highest detected exciton state in a semiconductor. In [3] excitons up to the main quantum number $n = 25$ were observed. As for a hydrogen atom the highly excited states are called *Rydberg excitons*.

The average radius $\langle r_n \rangle$ of an exciton with the main quantum number n and the angular momentum l is given by [4]

$$\langle r_n \rangle = \frac{1}{2} a_B \left(3n^2 - l \cdot (l+1)\right) \quad . \tag{13}$$

Due to the small effective mass and the resulting large Bohr radius Rydberg excitons have a large spatial extend ($\langle r_{25} \rangle = 1\,\mu m$). Rydberg excitons in Cu_2O have also a long lifetime (up to nanoseconds for high principal quantum numbers).

2 OPTICS

2.1 LINEAR OPTICS

In many systems the relation between the electric field $\mathbf{E}$ and the electric polarization $\mathbf{P}$ can be described by a linear equation

$$\mathbf{P} = \epsilon_0 \chi \mathbf{E} \ , \tag{14}$$

where χ is the electric susceptibility, which is a tensor of the second order. The theory of *linear optics* is based on this linear relation. The electric displacement field $\mathbf{D}$ is then defined by the equation

$$\mathbf{D} = \epsilon_0 \mathbf{E} + \mathbf{P} = \epsilon_0 \cdot (1 + \chi)\mathbf{E} = \epsilon_0 \epsilon_r \mathbf{E} \ . \tag{15}$$

2.1.1 *Electromagnetic Wave*

From now on a non magnetic medium ($\mu_r = 1$) with no free charges ($\rho_f = 0$) and current ($\mathbf{j} = 0$), which is suitable for e.g. dielectric materials, is assumed. The relation between the magnetic field strength $\mathbf{H}$ and the magnetic field is then given by the equation

$$\mathbf{B} = \mu_0 \mathbf{H} \ , \tag{16}$$

where μ_0 is the vacuum permeability.

A simple mathematical description for the propagation of light is given by a *plain wave*

$$\mathbf{E}(\mathbf{r}, t) = \mathbf{E}_0 \sin(\omega t - \mathbf{k} \cdot \mathbf{r}) \ , \tag{17}$$

which is a solution of the *Maxwell equations*

$$\text{div } \mathbf{D} = 0 \tag{18a}$$

$$\text{div } \mathbf{B} = 0 \tag{18b}$$

$$\text{rot } \mathbf{E} = -\frac{\partial \mathbf{B}}{\partial t} \tag{18c}$$

$$\text{rot } \mathbf{H} = \frac{\partial \mathbf{D}}{\partial t} \ . \tag{18d}$$

The absolute value of the *wave vector* $\mathbf{k}$

$$k = |\mathbf{k}| = \frac{\omega}{c} = \frac{2\pi}{\lambda} \tag{19}$$

and the angular frequency ω are not independent. The variable λ is called the *wavelength* and the constant

$$c = \frac{c_0}{n} = \frac{c_0}{\sqrt{\epsilon_r}} = \frac{1}{\sqrt{\mu_0 \epsilon_0 \epsilon_r}} \tag{20}$$

is the speed of light in the medium, where c_0 is the vacuum speed of light and n the refractive index.

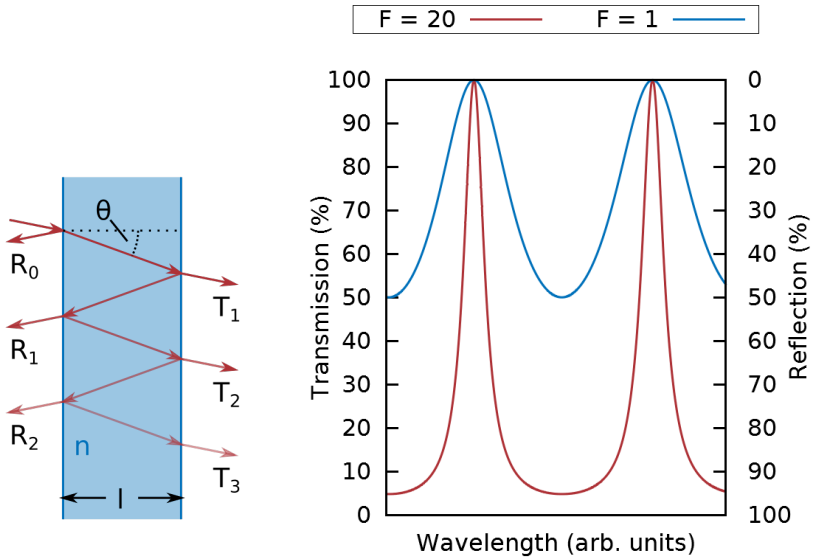

(a) Schematic picture.

(b) Transmission and reflection.

Figure 5: Fabry-Pérot Interferometer. a) Schematic picture of a typical Fabry-Pérot interferometer. A single beam of light enters the interferometer and is reflected and transmitted multiple times. The medium within the two surfaces has a refractive index n. b) The transmission and reflection of two Fabry-Pérot interferometers with finesses $F = 20$ (red) and $F = 1$ (blue) as functions of the wavelength λ.

2.1.2 *Fabry-Pérot Interferometer*

A *Fabry-Pérot interferometer* is built of two parallel partially reflective surfaces. Due to constructive and destructive interference only specific wavelengths can pass the interferometer without intensity reduction.

Figure 5a shows the layout of a typical Fabry-Pérot interferometer. The interferometer's transmission depends on the phase difference δ between two parallel beams (like T_1 and T_2 in Figure 5a). It can be calculated [5] that the transmission function is given by

$$T = \frac{(1-R)^2}{1+R^2-2R\cos(\delta)} = \frac{1}{1+F\sin\left(\frac{\delta}{2}\right)} \quad , \tag{21}$$

if both surfaces have a reflectance of R. The constant

$$F = \frac{4R}{(1-R)^2} \tag{22}$$

is the coefficient of finesse and describes the contrast between wavelengths of high and low transmission, as it can be seen in Figure 5b. In case of a perpendicular incidence ($\theta = 0$ in Figure 5a) the phase difference is given by

$$\delta = \frac{4\pi n l}{\lambda} \quad , \tag{23}$$

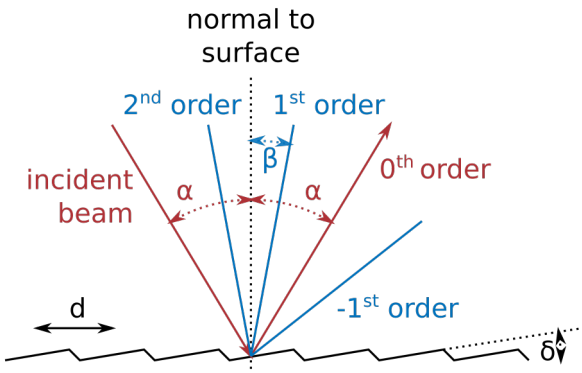

Figure 6: Reflection diffraction grating. An incident monochromatic light beam is reflected only in specific angles.

where l is the distance of the two surfaces and n the refractive index of the medium between them.

Figure 5b shows Equation 21 as a function of the wavelength λ for two different finesses. For the wavelengths, which fulfill the condition

$$\lambda = m2nl \tag{24}$$

for constructive interference, where m is an arbitrary integer, the transmission reaches the maximum ($T = 1$). The range between these maxima is called the free spectral range (FSR) $\Delta\lambda$.

2.1.3 *Grating*

An optical diffraction grating has a periodical structure and is able to split an incident light beam in its spectral components. Figure 6 shows a sketch of a *reflection diffraction grating*, which has a reflecting periodic surface structure.

Due to constructive and destructive interference an incident monochromatic beam of light is reflected only at specific angles. The grating equation, which determines the possible reflection angles, is given by

$$d \cdot (\sin(\alpha) + \sin(\beta)) = m\lambda \ , \tag{25}$$

where d is the periodical length of the structure, α respectively β the angle of the incident respectively the reflected light beam and the normal to surface, λ the wavelength and m an arbitrary integer. The reflection for $m = 0$ is called the 0th order, for $m = 1$ the 1st order and so on.

This equation neglects the specific structure of the surface (e.g. the angle δ in Figure 6) and only observes the periodical length. Certainly this specific structure determines the intensity of the reflections of the different orders.

A blazed grating is an optical diffraction grating, that can be tuned to maximize the intensity of a single diffraction order. In Figure 6 this can be achieved by setting $\delta = \beta$.

2.2 NONLINEAR OPTICS

In contrast to linear optics (see Section 2.1) *nonlinear optics* use higher orders of the electric susceptibility χ to describe the relation between the electric field $\mathbf{E}$ and the electric polarization $\mathbf{P}$

$$\mathbf{P} = \epsilon_0 \cdot \left(\chi^{(1)}\mathbf{E} + \chi^{(2)}\mathbf{E}^2 + \dots\right) \quad , \tag{26}$$

where $\chi^{(n)}$ are the *n^{th} order susceptibilities* of a medium. They are tensors of the order $n+1$.

2.2.1 *Second Harmonic Generation*

If a plane wave with an angular frequency ω incides a nonlinear medium the electric field $\mathbf{E}$ at the position $\mathbf{r} = 0$ is given by Equation 17

$$\mathbf{E}(t) = \mathbf{E}_0 \sin(\omega t) \quad . \tag{27}$$

For convenience only a single polarization

$$\mathbf{E}_0 = \mathbf{e}_x E_0 \tag{28}$$

is taken into account.

This leads to an electric polarisation of

$$\mathbf{P}(t) = \epsilon_0 \cdot \left(\chi_x^{(1)} E_0 \sin(\omega t) + \chi_{xx}^{(2)} E_0^2 \sin^2(\omega t)\right) \quad , \tag{29}$$

if only the first two terms of Equation 26 are taken into account.

Using the trigonometric identity

$$\sin^2(x) = \frac{1}{2} - \frac{\cos(2x)}{2} \tag{30}$$

leads to the electric polarization

$$\mathbf{P}(t) = \epsilon_0 \cdot \left(\frac{1}{2}\chi_{xx}^{(2)} E_0^2 + \chi_x^{(1)} E_0 \sin(\omega t) - \frac{1}{2}\chi_{xx}^{(2)} E_0^2 \sin^2(2\omega t)\right) \tag{31}$$

with a term

$$-\frac{1}{2}\chi_{xx}^{(2)} E_0^2 \sin^2(2\omega t) \tag{32}$$

oscillating at the frequency 2ω. This leads to a generation of a plane wave with twice the frequency of the original one. The effect is called the *second harmonic generation*.

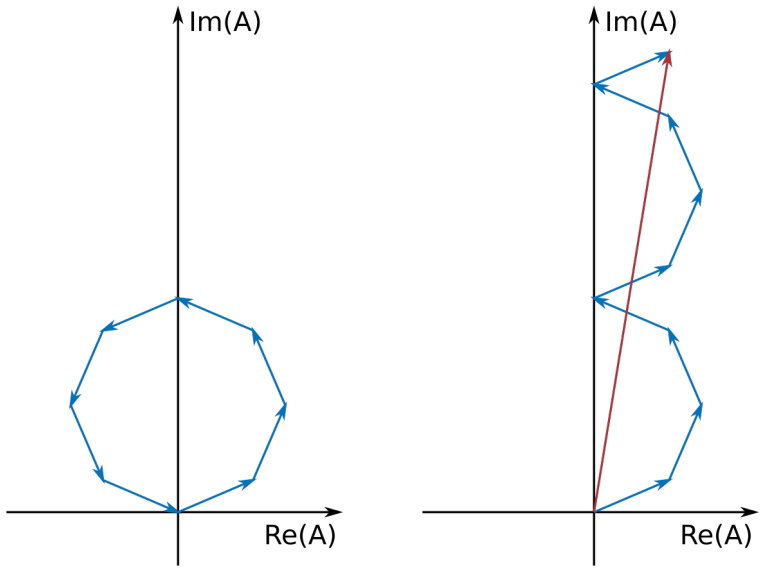

(a) No phase matching. (b) Quasi-phase matching.

Figure 7: Difference between no and quasi-phase matching. [6] The blue arrows symbolize the amplitude and phase of the generated wave; the red arrow stands for the corresponding propagating wave. a) Without phase matching the amplitude of the propagating wave oscillates between zero and the maximum. b) With quasi-phase matching the intensity of the propagating wave increases continuously, since the phase of newly generated frequency components is flipped after a cycle.

2.2.2 *Quasi-Phase Matching*

The absolute value of the wave vector of a plane wave is given by

$$k(\omega) = |\mathbf{k}(\omega)| = \frac{2\pi}{\lambda} = \frac{\omega n(\omega)}{c_0} \quad , \tag{33}$$

where $n(\omega)$ is the refractive index at the angular frequency ω and c_0 the vacuum speed of light.

While for the generated second harmonic wave it holds that $k_{gen} = 2k(\omega)$, a propagating wave has an absolute value of the wave vector of $k_{prop} = k(2\omega)$. This leads to a *phase mismatch*

$$\Delta k = k_{prop} - k_{gen} = k(2\omega) - 2k(\omega) = \frac{2\omega}{c_0}(n(2\omega) - n(\omega)) \tag{34}$$

between the generated and the propagating second harmonic, because usually the refractive indices differ for different frequencies.

Figure 7a shows the consequence of the phase mismatch. Instead of increasing the intensity of the propagating wave oscillates. The distance between the minimum and maximum intensity in the crystal is called the *coherence length*.

In Figure 7b the nonlinear interaction of the medium is reversed every coherence length. Thus the intensity of the propagating second harmonic increases continuously. This concept is called *quasi-phase matching*.

The coherence length depends on the wavelengths and the refractive indices of the medium. By changing the temperature the refractive indices usually change. Thereby it is possible to achieve constant coherence lengths for different wavelengths by changing the temperature. This is necessary for quasi-phase matching over a wide range of wavelengths with a single crystal.

2.3 LASERS

Light amplification by stimulated emission of radiation (laser) is a process of optical amplification of light. A laser is built of an optical *resonator* and a *gain medium*. The gain medium needs energy for the light amplification. This process is called pumping and can be done by e.g. light or electric current.

A laser can emit light either continuously (CW) or pulsed. Due to the *energy-time uncertainty principle* a pulsed laser has a very broad spectrum. If a very narrow spectrum is necessary, a laser operating in CW is needed.

2.3.1 *Laser Diode*

A *laser diode* uses a p-n junction of a semiconductor as the gain medium. Laser diodes are compact, cost effective and efficient. In contrast to a light-emitting diode (LED) a laser diode emits laser light due to the additional resonator. The power of the a laser diode can be easily controlled through the electric current.

Without an external resonator laser diodes have a broad emission spectrum and tend to mode hopping. They are also unstable due to temperature changes.

The laser diode used in this experiment has an anti-reflection (AR) coating to weaken the mode selection of the internal resonator. It is not able to lase without an external feedback, which is advantageous for wavelength tuning. The resonator then forms a Fabry-Pérot interferometer with a very small finesse (see Equation 22).

Varying the temperature of the laser diode changes the refractive index and the length of the resonator, which modifies the resulting gain profile (see Equation 23). Changing the laser diode's current alters the temperature of the laser diode with the same consequences. However there is an additionally modification of the refractive index due to the higher or lower charge density at the p-n junction.

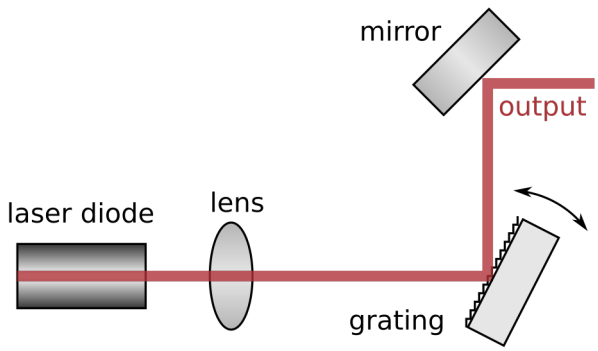

Figure 8: Littrow configuration. [7] In the Littrow configuration a diffractive reflection grating is used as the wavelength selective optical element.

2.3.2 *Littrow ECDL*

An external-cavity diode laser (ECDL) uses an additional external resonator with wavelength selective elements to stabilize and tune the mode selection. A possible realization of an ECDL is the Littrow configuration, which is shown in Figure 8.

The Littrow ECDL uses an AR-coated laser diode and a blazed diffraction reflection grating. The grating is optimized to reflect the first reflection order back into the laser diode. The lens is necessary to focus the light onto the diode's surface. By turning the grating the reflection condition is fulfilled for different wavelengths and offers the possibility of tuning the wavelength.

The 0th order reflection beam is used as the output beam. Its direction changes depending on the grating angle. To compensate the grating dependent output beam direction, additional optics are necessary, which is hinted by the mirror in Figure 8.

Figure 9 shows the mode selection of a Littrow ECDL. For a coarse tuning of the wavelength it is sufficient to turn the grating.

The profile of the grating is very broad compared to the external and internal modes. Therefore the effect of the grating is not dominating for fine wavelength tuning.

The external modes shift by turning the grating due to the changed resonator length. If the internal modes are held constant, the wavelength can be tuned continuously only about the distance between two external modes. By exceeding this limit the wavelength hops to another wavelength with another external mode. The maximum range of tuning the wavelength continuously is called the *mode-hop free tuning range*.

The mode-hop free tuning range can be increased by varying not only the external modes but also the internal modes. This can be achieved by changing the electric current simultaneously to the grating angle. This process is called *feed forward*. Unfortunately this leads

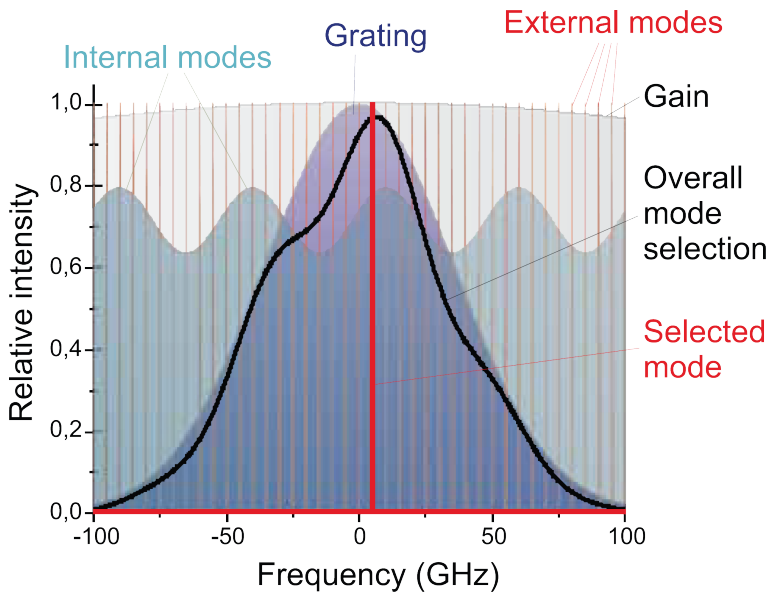

Figure 9: Mode selection of a Littrow ECDL. [7] The mode selection depends on the external modes, the grating, the internal modes and the gain.

to a wavelength dependent intensity, because through the electric current also the gain is changed. Varying the electric current furthermore changes the temperature of the laser diode and consequently the internal modes.

3 SPECTROSCOPY

Spectroscopy is among others the analysis of the electromagnetic spectra of substances. In this thesis the transmission spectrum of Cu_2O is investigated.

3.1 LINEWIDTH

A particle in the lower of two different energy states can absorb a photon that has the same energy as the difference between the two states. The transmission spectrum of these particles shows then an absorption dip around this energy.

Figure 10 sketches a possible transmission spectrum of a two state particle. The width of the absorption line is called *linewidth*. There are several physical effects, that can broaden the absorption line.

One effect is the uncertainty principle. The relation between the lifetime τ and the linewdith Γ is given by the equation

$$\Gamma\tau = \hbar \ . \tag{35}$$

The relation between the thickness L of a sample and the transmitted power P_T is given by the *Lambert-Beer law*

$$P_T = P_0 e^{-\alpha L} = P_0 e^{-\tau} \ , \tag{36}$$

where α is the absorption coefficient, P_0 the power of the laser, before it incides the sample, and $\tau = \alpha L$ the *optical depth*.

The frequency dependent absorption coefficient α has a *Lorentzian profile*

$$\alpha(E, \Delta E) = C \frac{\frac{\Gamma}{2}}{\left(\frac{\Gamma}{2}\right)^2 + (E - \Delta E)^2} \ , \tag{37}$$

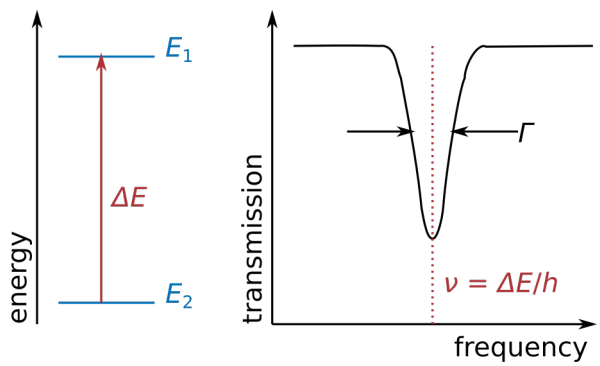

Figure 10: Absorbtion spectrum of a particle with two energy states.

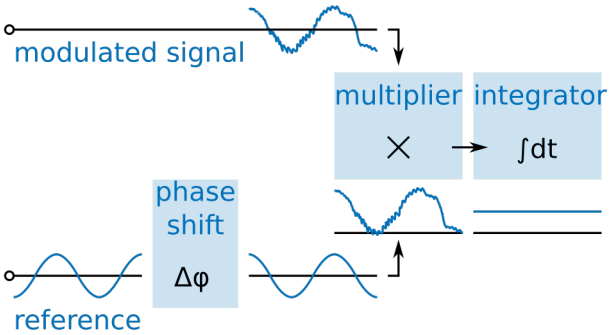

Figure 11: Operating principle of a simple lock-in amplifier.

where C is a constant of proportionality.

Due to phonon-assisted absorption the symmetric Lorentzian profile has to be adjusted. Therefore, the asymmetric Lorentzian profile

$$\alpha(E, \Delta E) = C \frac{\frac{\Gamma}{2} + 2q \cdot (E - \Delta E)}{\left(\frac{\Gamma}{2}\right)^2 + (E - \Delta E)^2} \quad , \tag{38}$$

where the variable q describes the asymmetry, is used.

3.2 MODULATION SPECTROSCOPY

With modulation spectroscopy one or several parameters of the light, that is used for the spectroscopy, is modulated with a fixed and known frequency before it incides the sample. The detector's signal can then be analyzed under consideration of the known modulation frequency. The huge advantage of modulating the signal is, that eventual disruptive influences (noise, constant offset) have a specific frequency range. By modulating the signal outside this range, which is often fulfilled for high modulation frequencies, the validity of the measured signals can be significantly increased.

3.2.1 *Lock-In Amplifier*

A *lock-in amplifier* is an amplifier that separates the amplitude of a modulated signal at a distinct known frequency from a noisy background [8]. Figure 11 shows the operating principle of a lock-in amplifier:

A modulated signal U_{in} is multiplied with a sinusoidal reference signal, that has the exact same frequency f as the modulation of the modulated signal. Subsequently the resulting signal is integrated over a time T, that is much longer than the period of the modulation. The resulting DC signal U_{out} has a much higher signal-to-noise ratio (SNR). As an advantage a lock-in amplifier filters DC signals or signals, which

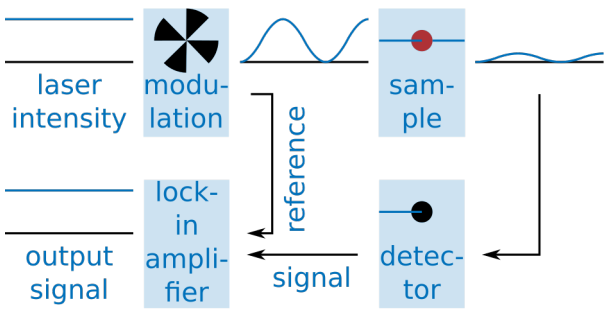

Figure 12: Simple amplitude modulation setup.

frequency differs from the reference signal's frequency. Hence, eventual noise in a signal is eliminated by the lock-in amplifier except for the particular noise component at the modulation frequency. The phase shift is necessary to adjust the phase of modulated and reference signal.

Mathematically the output signal U_{out} can be described by the equation

$$U_{out}(t) = \frac{1}{T} \int_{t-T}^{t} \sin(2\pi f t' + \Delta\phi) U_{in}(t')\, dt' \ . \tag{39}$$

Sine functions and respectively cosine functions with different frequencies are orthogonal to each other. Also a sine and a cosine function with the same frequency are orthogonal. Due to these relations only a signal with the right frequency and phase can pass the lock-in amplifier.

3.2.2 *Amplitude Modulation Spectroscopy*

Figure 12 shows a simple setup for an *amplitude modulation spectroscopy*: The laser beam is guided through a chopper, which is connected to the reference input of the lock-in amplifier. The laser beam then has a modulated intensity that passes the sample. The power of the transmitted laser beam can be measured by a photo diode, which is connected to the signal input of the lock-in amplifier. The output signal of the lock-in amplifier is proportional to the mean transmitted laser beam power.

This setup can extract the pure modulated transmitted laser power from the noisy background of the signal and can thus increase the SNR of the signal. The origin of the background noise can be optical (e.g. background light and laser noise) or electronic (e.g. by the detector and amplifier).

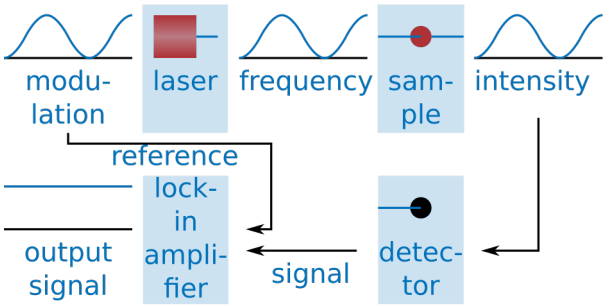

Figure 13: Simple frequency modulation setup.

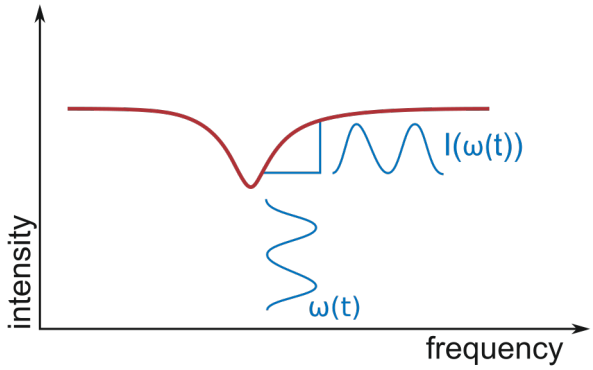

Figure 14: Principle of frequency modulation spectroscopy. The modulated laser frequency leads to a modulated intensity behind the sample. This modulated intensity can be analyzed using a lock-in amplifier and can be interpreted as the 1st derivative of the absorption coefficient.

3.2.3 *Frequency Modulation Spectroscopy*

Another method of modulation spectroscopy is the so called frequency modulation (FM) spectroscopy. Instead of the amplitude the wavelength of the laser is modulated. Figure 13 shows a possible simple setup for this: The frequency of a tunable laser source is modulated. In the present setup this can be achieved by driving a piezo-electric crystal, which is linked to the grating in the resonator, with a sinusoidal voltage. The piezo voltage's trigger signal is used as the reference for a lock-in amplifier. The frequency modulated laser beam passes the sample, which adds a modulation to the amplitude of the laser beam (see Figure 14). This amplitude modulated laser beam is detected by a photo diode, whose voltage is used as the signal for the lock-in amplifier. The demodulated signal can be interpreted as the 1st derivative of the absorption coefficient α.

For the derivation of the last interpretation only a few physical laws are necessary: The transmitted power $P_T(\omega)$ can be approximated using the Taylor formula

$$\begin{aligned} f(x) \overset{x\to x_0}{\approx} & f(x_0) + f'(x_0)(x-x_0) + \frac{f''(x_0)}{2}(x-x_0)^2 \\ & + \frac{f'''(x_0)}{6}(x-x_0)^3 \end{aligned} \tag{40}$$

around the a central frequency ω_0

$$\begin{aligned} P_T(\omega) \overset{\omega\to\omega_0}{\approx} & P_T(\omega_0) + P_T'(\omega_0)(\omega-\omega_0) + \frac{P_T''(\omega_0)}{2}(\omega-\omega_0)^2 \\ & + \frac{P_T'''(\omega_0)}{6}(\omega-\omega_0)^3 \quad . \end{aligned} \tag{41}$$

With a sinusoidal frequency modulation ($\omega(t) = \omega_0 + A\sin(\Omega t)$) the last equation becomes

$$\begin{aligned} P_T(t) \overset{\omega\to\omega_0}{\approx} & P_T(\omega_0) + P_T'(\omega_0)A\sin(\Omega t) + \frac{P_T''(\omega_0)}{2}A^2\sin(\Omega t)^2 \\ & + \frac{P_T'''(\omega_0)}{6}A^3\sin(\Omega t)^3 \quad . \end{aligned} \tag{42}$$

The approximation of the Lambert-Beer law (see Equation 36) for thin layers ($\alpha(\omega)\cdot L = \tau \ll 1$) is given by

$$P_T = P_0(\omega)e^{-\alpha(\omega)L} \approx P_0(\omega)\,(1-\alpha(\omega)L) \quad . \tag{43}$$

With the assumption $P_0(\omega) = P_0(\omega_0)$ (no amplitude modulation) it holds with Equation 43

$$\left(\frac{d^n}{d\omega^n}P_T\right)\bigg|_{\omega_0} = -P_0(\omega_0)L\left(\frac{d^n}{d\omega^n}\alpha\right)\bigg|_{\omega_0} \tag{44}$$

for the derivatives of the transmitted power. Inserting Equation 44 in Equation 42 leads to

$$\begin{aligned} P_T(t) \approx & P_T - P_0(\omega_0)L\alpha'(\omega_0)A\sin(\Omega t) \\ & - P_0(\omega_0)L\frac{\alpha''(\omega_0)}{2}A^2\sin^2(\Omega t) \\ & - P_0(\omega_0)L\frac{\alpha'''(\omega_0)}{6}A^3\sin^3(\Omega t) \quad . \end{aligned} \tag{45}$$

Using two trigonometric identities

$$\sin^2(x) = \frac{1}{2}\left(1-\cos(2x)\right) \tag{46a}$$

$$\sin^3(x) = \frac{1}{4}\left(3\sin(x) - \sin(3x)\right) \tag{46b}$$

Equation 45 gets to

$$\begin{aligned} P_T(t) \approx & P_T - P_0(\omega_0) L \alpha'(\omega_0) A \sin(\Omega t) \\ & - P_0(\omega_0) L \frac{\alpha''(\omega_0)}{2} A^2 \frac{1}{2} (1 - \cos(2\Omega t)) \\ & - P_0(\omega_0) L \frac{\alpha'''(\omega_0)}{6} A^3 \frac{1}{4} (3 \sin(\Omega t) - \sin(3\Omega t)) \end{aligned} \tag{47}$$

Sorting the last equation by the different harmonics of modulation and by dividing it by $P_0(\omega_0)$ leads to

$$\begin{aligned} \frac{P_T(t)}{P_0(\omega_0)} \approx & (1 - \alpha(\omega_0) L) - A^2 L \frac{\alpha''(\omega_0)}{4} \\ & + \left(-AL\alpha'(\omega_0) - A^3 L \frac{\alpha'''(\omega_0)}{8} \right) \sin(\Omega t) \\ & + A^2 L \frac{\alpha''(\omega_0)}{4} \cos(2\Omega t) \\ & + A^3 L \frac{\alpha'''(\omega_0)}{24} \sin(\Omega t) \ . \end{aligned} \tag{48}$$

If there is only a small modulation amplitude A the harmonics of modulation correspond to the derivatives of the absorption coefficient α.

A simultaneous amplitude modulation leads to additional terms in Equation 44. The demodulated signal is shifted by a constant proportional to the amplitude of the amplitude modulation. This effect can be potentially reduced by using balanced detectors.

Part II

EXPERIMENT

4 SETUP

Figure 15 shows the experimental setup. A frequency doubled laser beam is amplitude modulated and passes the sample in the cryostat. It is subsequently detected by a photo diode. The following subsections will explain the setup in detail.

4.1 TUNABLE DIODE LASER

For this experiment a Toptica DL Pro is used, which is a Littrow ECDL. It has a linewidth of less than 1 MHz [9] and operates at a power of less than 80 mW. The wavelength is tuned between about 1140 nm and 1141 nm. The coarse tuning ($> 0.1\,nm$) can be achieved by mechanical turning of the grating with a screw. For the fine tuning ($< 0.1\,nm$) a piezo-electric crystal can be used that can turn the grating much more precisely. The accessible mode hop-free tuning range should be greater than 20 GHz. The output beam is linear polarized and has a diameter of $3\,mm \times 1\,mm$ [9]. To correct the ellipticity of the laser beam an anamorphic prism pair (APP, Thorlabs PS883-C) is used.

4.2 WAVEGUIDE

For the second harmonic generation a 20 mm long periodically poled MgO doped lithium niobate (MgO:PPLN) waveguide is used. It is embedded in a waveguide with several channels. The waveguide has a normalized conversion efficiency of 140%/W/cm² and a poling period of 8.68 µm. It has an AR-coating of $R < 0.5\,\%$ (571 nm) respectively $R < 0.3\,\%$ (1142 nm).

Due to the periodic poling quasi-phase matching can be achieved. To tune the phase matching condition to different wavelengths the waveguide is placed on a copper block temperature controlled by a heater (Thorlabs TC200-EC). For the coupling a 20x microscope objective is used, which is mounted on a 3-axis stage (Thorlabs MDT616). The maximum SHG efficiency is about 10 %.

4.3 FILTER, NOISE EATER AND SPECTRUM ANALYZER

One part of the laser beam, which is splitted by a polarized beam splitter, is guided with an optical fiber (Thorlabs P1-SMF28E-FC-6) to a spectrum analyzer (ANDO AQ-6315E optical spectrum analyzer). Unfortunately the spectrum analyzer has an absolute shift of about

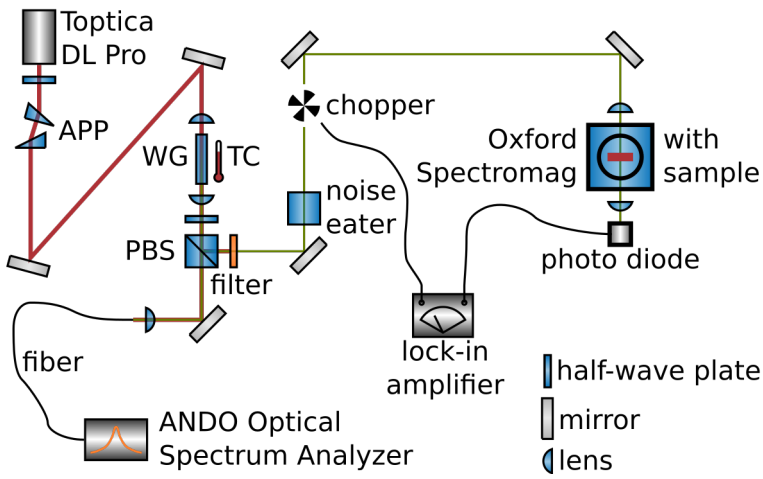

Figure 15: Scheme of the experimental setup with the abbreviations anamorphic prism pair (APP), waveguide (WG), temperature controller (TC) and polarizing beamsplitter (PBS.)

0.3 nm, so that only relative relations between measurement points can be determined with a sufficient resolution.

The other part of the beam passes a filter (Thorlabs FB570-10) to get rid of the original infrared part (around 1141 nm) of the laser spectrum. The noise eater (Thorlabs LCC3111L/M) stabilizes and controls the power of the laser.

4.4 CHOPPER, PHOTO DIODE AND LOCK-IN AMPLIFIER

The chopper (HMS Light Beam Chopper 220A) modulates the intensity of the laser beam with a frequency of about 3 kHz. The laser beam is then guided through the cryostat, passes the sample and gets detected by a Si amplified detector (Thorlabs PDA100A-EC). The signal of the chopper is used as the reference signal for a lock-in amplifier (Zurich Instruments UHFLI), whereas the detector signal is used as the lock-in input signal.

4.5 CRYOSTAT

In this experiment an Oxford Spectromag cryostat is used. During the experiment stable temperatures down to 1.7 K are achieved. The optical access is enabled through a few Mylar films. Unfortunately these films are not perfectly clean with the result, that most of the laser intensity (about 90 %) is reflected, absorbed or scattered by these films. The light beam is focused on the sample through a lens ($f = 200\,\mathrm{mm}$) and afterwards collected by a second lens ($f = 50\,\mathrm{mm}$). The high focal length of the second lens is chosen to collect in addition to the laser beam itself a lot of scattered laser light on the detector.

Figure 16: Sample holder with two samples. The left sample is a 70 µm thick Cu_2O crystal from Russia. The right one is an artificial 100 µm thick sample from the Max Planck Institute For Solid State Research.

4.6 SAMPLES

Figure 16 shows the sample holder with two strain-free mounted polished Cu_2O crystals. The left sample is 70 µm thick and from Russia; the right one is a 100 µm artificially grown crystal from the Max Planck Institute for Solid State Research (MPI). Our third crystal is also from the MPI and is a bit thicker than the 100 µm crystal. From all of our crystals only the artificially 100 µm thick one shows absorption lines due to exciton transitions.

5 METHOD OF MEASUREMENT

For the first measurements no modulation spectroscopy was applied. Due to the low detected intensity the SNR was to low for acceptable results. Therefore two concepts of modulation spectroscopy were implemented and tested. Of these two methods only the amplitude modulation spectroscopy yields good results.

5.1 AMPLITUDE MODULATION SPECTROSCOPY

Every data point of the spectrum is measured manually. By turning the grating and varying the piezo voltage the right wavelength for the second harmonic is set. With the used spectrum analyzer this can be done with a resolution of up to 0.002 nm. When necessary the temperature of the waveguide and the coupling into the fiber is optimized to get at least a power of the SHG higher than 500 µW.

The noise eater output power is set to 300 µW. The LED of the noise eater can then be used as an indicator for the necessity of coupling or temperature optimization, since it turns red, if the input power is too low. Otherwise it shines green.

This chosen power levels appear to be a good compromise. A high output power is advantageous for the detection of the transmitted laser power. On the other hand reduces a lower laser power the need of tuning the wavelength, because even a low coupling efficiency can be sufficient.

The chopper runs with a frequency of about 3 kHz. The temperature of the cryostate is set to a stable temperature between 1.7 K and 2.1 K. The demodulated detector signal with and without a sample is noted. The integration time of the lock-in amplifier is set to 1 s. For the Si amplified detector an amplification of 50 dB is used.

This procedure has to be repeated for each data point.

5.2 FREQUENCY MODULATION SPECTROSCOPY

The frequency modulation spectroscopy is realized by a modulated voltage at the piezo-electric crystal with a frequency of about 1 kHz. For a continuous frequency modulation the wavelength has to stay within the mode-hop free tuning range. Therefore the laser has to be tuned around the central frequency by varying the electric current, the temperature, the feed forward parameter and the piezo voltage.

Unfortunately, the essential feed forward leads to an additional amplitude modulation. Since modulation spectroscopy works best at

high frequencies, the noise eater is not able to compensate this amplitude modulation. This is why the demodulated signal cannot be interpreted directly as the 1st derivative of the absorption coefficient. Normally this leads only to an additional offset, that can be ignored or subtracted afterwards.

Also the second condition (see Equation 43) of the derivation in Section 3.2.3 is not fulfilled: A sample thickness of $L = 100\,\mu m$ is to large for the approximation $\alpha L = \tau \ll 1$. The measured optical depths were usually between 4 and 7. This leads to the situation, that the demodulated signal can not be directly interpreted as the 1st derivation of the absorption coefficient.

For this method of measurement we were not able to reduce the noise of the demodulated signal to an acceptable value. The fluctuations were to high to note only a single value with a sufficient accuracy.

Part III

RESULTS

6 LASER

In this experiment a Toptica DL Pro (Littrow ECDL) is used. The laser has a specific power and a specific wavelength. In the next sections the influence of temperature, current and piezo voltage on the parameters power and wavelength are investigated.

6.1 POWER

6.1.1 *Influence of Current*

Figure 17 shows the influence of the current on the power of the laser. The temperature is set to the constant value $T_{set} = 20.0\,°C$. Also the grating angle is fixed. The power is measured using a Ge photodiode (Thorlabs S122C).

The measurement data are fitted with the function

$$P(I) = m \cdot I - c \quad . \tag{49}$$

For the fit constants the values $m = (507 \pm 4)\,\mu W\,mA^{-1}$ and $c = (33.6 \pm 0.6)\,mW$ are determined.

The laser starts lasing, when the current exceeds the threshold $I_{thresh} = (66 \pm 2)\,mA$. From this value on the power increases linear to the electric current.

By varying the electric current the dominating process regarding the output power is the changed gain of the laser diode. The variation of the internal modes with respect to the power is negligible, but it is of importance for the wavelength behavior.

6.1.2 *Influence of Temperature*

In Figure 18 the power of the laser is plotted for different temperatures, while both electric current ($I_{set} = 190\,mA$) and grating angle are held constant.

The measured power increases linearly with increased temperature. Therefore the measurement data are fitted with a linear function

$$P(T) = -m \cdot T + c \quad . \tag{50}$$

The fit parameters have the values $m = (1.17 \pm 0.07)\,mW\,°C^{-1}$ and $c = (78 \pm 2)\,°C$.

In contrast to the situation in the last subsection, the change of the internal modes with temperature variations, is not negligible. This is why the measured powers at some points depart conspicuously from the ideal linear function.

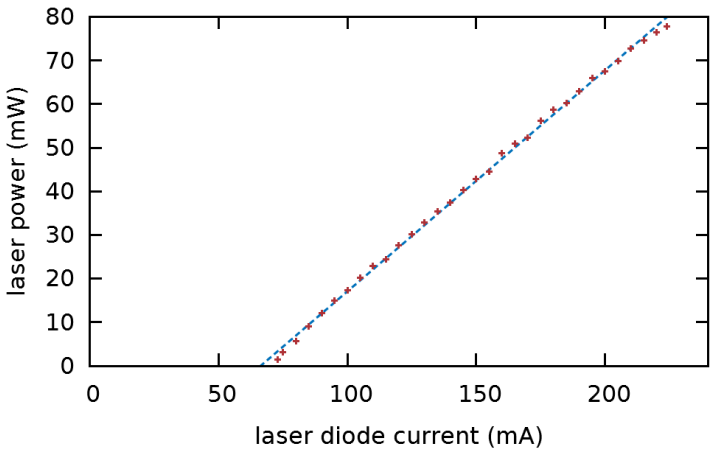

Figure 17: Influence of current on the power. Temperature ($T_{set} = 20.0\,°C$) and grating angle are held constant. The power is measured with a Ge photo diode (Thorlabs S122C). The measurement data (red) are fitted with a linear function (blue) $P(I) = 507\,\mu W\,mA^{-1} \cdot I - 33.6\,mW$.

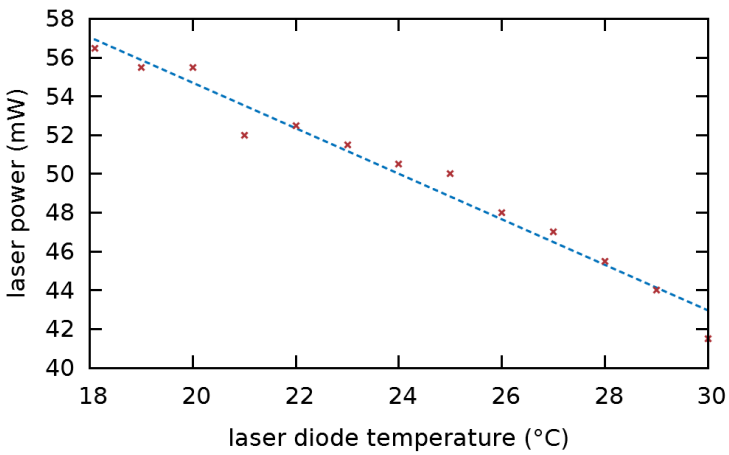

Figure 18: The influence of the temperature on the laser power. Current ($I_{set} = 190\,mA$) and grating angle are held constant. The power is measured with a Ge photo diode (Thorlabs S122C). The measured data (red) are fitted with a linear function (blue) $P(T) = -1.17\,mW\,°C^{-1} \cdot T + 78\,mW$.

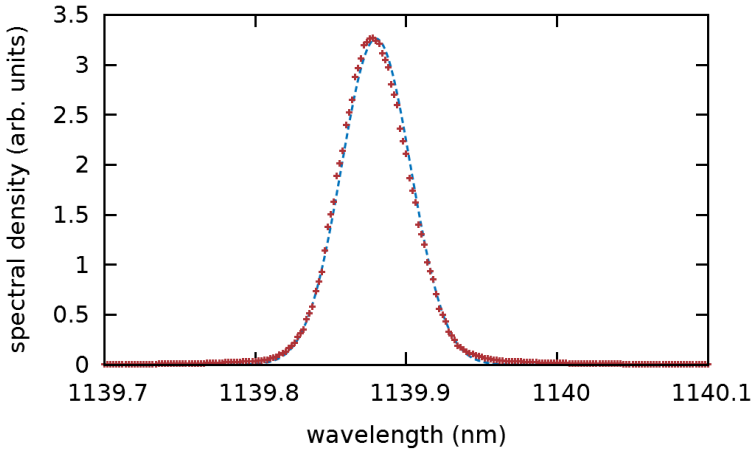

Figure 19: Spectrum of the laser. The current is set to $I_{set} = 170\,mA$ and the temperature to $T_{set} = 20.0\,°C$. The spectrum is taken with an ANDO AQ-6315E optical spectrum analyzer. The measurement data (red) is fitted with a Gaussian function (blue) $S(\lambda)$. The linewidth is due to limitations of the optical spectrum analyzer much greater than the real linewidth of the laser.

6.2 SPECTRUM

Figure 19 shows a typical laser spectrum. The spectral density S is fitted with a Gaussian function

$$S(\lambda) = a \cdot \exp\left(-\frac{(\lambda - b)^2}{2c^2}\right) \tag{51}$$

with the fit parameters $a = 3.26 \pm 0.02$, $b = (1139.880 \pm 0.005)\,nm$ and $c = (0.0229 \pm 0.0001)\,nm$.

The first variable a is only for the normalization. The second variable b is the central frequency of the laser. The parameter c is proportional to the linewidth $FWHM = 2\ln(2)c \approx 2.35c = 0.054\,nm$, where FWHM is the full width at half maximum. The measured linewidth (about 12 GHz) is much greater than the real linewidth of the laser beam (about 1 MHz) due to limitations of the spectrum analyzer.

For the following discussions only the central wavelength is of importance.

6.2.1 *Influence of Temperature*

Figure 20 shows the influence of the laser diode's temperature on the wavelength. The graph shows a linear relation between the temperature and the laser wavelength in the investigated temperature range. However the wavelength variation is not homogeneous due to mode-hops.

The measurement data is fitted with a linear function

$$\lambda(T) = m \cdot T + c \ . \tag{52}$$

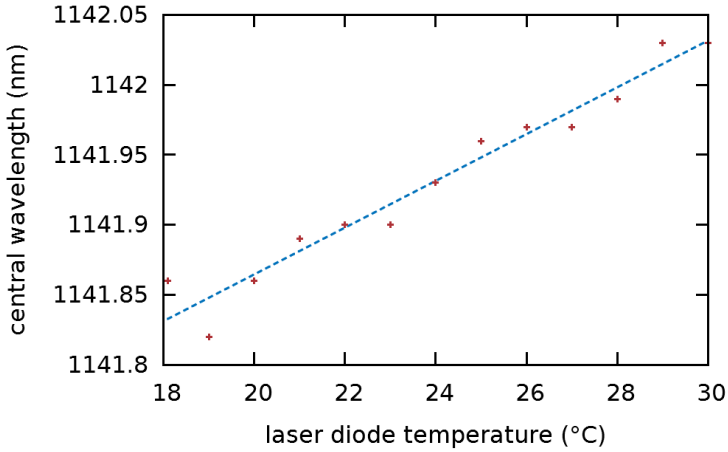

Figure 20: The influence of the temperature on the central wavelength. Both current ($I_{set} = 190\,mA$) and grating angle are held constant. The wavelength is determined with an ANDO AQ-6315E optical spectrum analyzer. The measurement data (red) are fitted with a linear function (blue) $\lambda(T) = 17\,pm\,°C^{-1} \cdot T + 1141.53\,nm$.

For the fit constants the values $m = (17 \pm 2)\,pm\,°C^{-1}$ and $m = (1141.53 \pm 0.03)\,nm$ were determined.

6.2.2 *Influence of Piezo Voltage*

Figure 21 shows the influence of the piezo voltage on the central wavelength of the laser. Since there are possible mode-hops the measurement data differ clearly from a perfect straight line.

For the fit a linear function

$$\lambda(U) = -m \cdot U + c \tag{53}$$

is used. The fit parameters are $m = (2.80 \pm 0.08)\,pm\,V^{-1}$ and $c = (1142.080 \pm 0.006)\,nm$.

6.3 MODE-HOP FREE TUNING

With mode-hop free tuning it is possible to tune the wavelength of the laser continuously. This allows to tune the laser wavelength with an accuracy higher than the spectrum analyzer's resolution. Also it is essential for the frequency modulation spectroscopy.

6.3.1 *Indicators*

The direct discontinuity of the wavelength because of mode-hops is poorly detectable with the used spectrum analyzer due to the limited sampling rate and resolution. Therefore another effect for the detection of mode-hops is used:

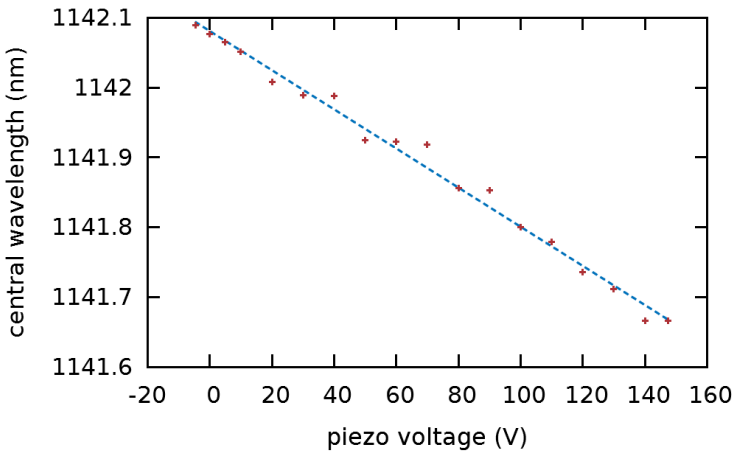

Figure 21: Voltage's influence on the central wavelength (with mode-hops). Both current ($I_{set} = 190\,mA$) and temperature ($T_{set} = 20.0\,°C$) are held constant. The wavelength is determined with an ANDO AQ-6315E optical spectrum analyzer. The measurement data (red) are fitted with a linear function (blue) $\lambda(U) = -2.8\,pm\,V^{-1} \cdot U + 1142.080\,nm$.

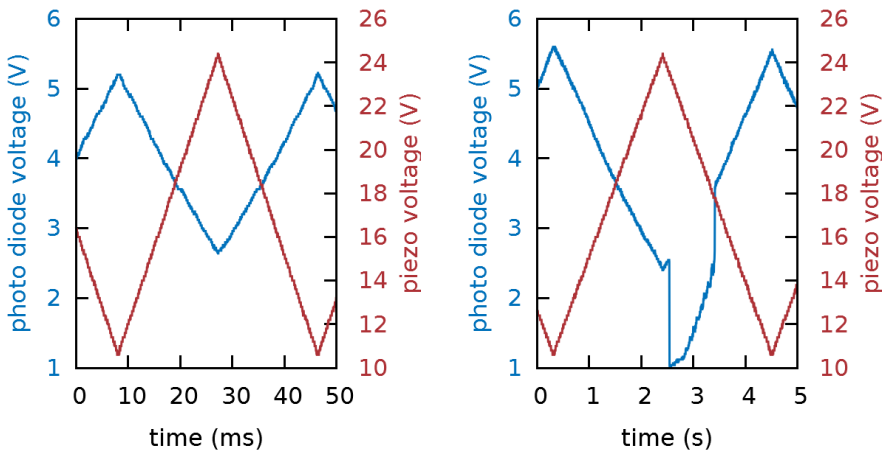

(a) $f = 26.0\,Hz$.

(b) $f = 0.24\,Hz$

Figure 22: Difference of the mode-hop free tuning range between low and high modulation frequencies f. The piezo electric crystal is driven by a symmetric ramp voltage (red). The blue measurement points show the voltage measured at the photo diode.

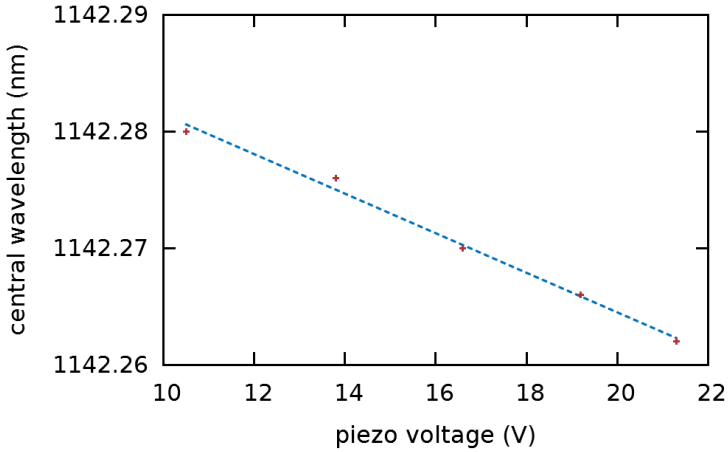

Figure 23: Influence of the voltage on the wavelength (mode-hop free). The temperature ($T_{set} = 21.5\,°C$) is held constant, while the electric current I_{set} varies because of the feed forward. The wavelength is determined with an ANDO AQ-6315E optical spectrum analyzer. The laser is mode-hop free tuned within this voltage range. The measurement data (red) are fitted with a linear function (blue) $\lambda(U) = -1.70\,pm\,V^{-1} \cdot U + 1142.300\,nm$.

If a wavelength mode-hop occurs while changing the piezo voltage, usually but not always this leads also to a significant discontinuity in the power of the laser. This can be easily detected with a photo diode even at high frequencies.

Figure 22a shows a well mode-hop free tuned laser, while in Figure 22b a mode-hop is clearly visible. Also the figures show the influence of the feed-forward, that prevents a piezo voltage independent laser power.

The mode-free tuning range can be optimized by varying the parameters current, temperature, piezo voltage and the feed-forward parameter.

6.3.2 *Properties*

Figure 23 shows the influence of the voltage on the wavelength within the mode-hop free range. The measurement data are fitted with a linear function

$$\lambda(U) = -m \cdot U + c \ . \tag{54}$$

For the fit constants the values $m = (1.70 \pm 0.09)\,pm\,V^{-1}$ and $c = (1142.300 \pm 0.002)\,nm$ are determined.

The slope ($m = (1.70 \pm 0.09)\,pm\,V^{-1}$) of the mode-hop free tuned laser is much less than the slope ($(2.80 \pm 0.08)\,pm\,V^{-1}$) of the mode-hoping laser (see Figure 21 and Equation 6.2.2).

6.3.3 *Influence of Frequency*

Figure 22 shows, that the mode-hop free tuning range depends on the modulation frequency of the piezo voltage, while the other parameters are hold constant. The mode hop-free tuning range is significantly smaller for low frequencies.

A possible explanation for this behavior is the influence of the diode's temperature on the internal modes: For high modulation frequencies the temperature change based on the modulated current is negligible, because the cycle duration is to short to heat the diode significantly. The modification of the internal modes is only affected by the change of the refractive index due to the change of the charge density at the p-n junction.

With low modulation frequencies the cycle duration is long enough to change the diode's temperature, but too fast to be compensated by the laser's PID temperature controller. This explains also the asymmetry in Figure 22b. For low frequencies the internal modes are changed both by charge density at the p-n junction and temperature changes and complicate a mode-hop free tuning.

7 WAVEGUIDE

To fulfill the quasi-phase match condition for different wavelengths, the temperature of the waveguide is varied. Figure 24 shows the temperatures of the waveguide in dependence of the wavelength. It also shows the theoretical exciton states for the corresponding second harmonic of each wavelength, which converge to the band gap energy around 1141.66 nm (SHG: 570.83 nm).

For the fit a linear function

$$T(\lambda) = m \cdot \lambda - c \tag{55}$$

is used. The fit parameters are $m = (11.12 \pm 0.07)\,°\mathrm{C}\,\mathrm{nm}^{-1}$ and $c = (12\,650 \pm 80)\,°\mathrm{C}$.

The conversion efficiency is about 7.4 %. This is an acceptable value, although the theoretical 10 % efficiency as specified by the manufacturer is not reached. It depends significantly on the chosen waveguide temperature. A temperature mismatch of only 1 °C can reduce the efficiency by half.

Also the position and alignment of the waveguide and the polarization of the laser beam affect the conversion efficiency.

Figure 25 shows the spectrum of the SHG behind the waveguide. The data are fitted with a Gaussian function

$$S(\lambda) = a \cdot \exp\left(-\frac{(\lambda - b)^2}{2c^2}\right) \tag{56}$$

with the fit parameters $a = (211 \pm 2) \cdot 10^{-6}$, $b = (569.964 \pm 0.006)\,\mathrm{nm}$ and $c = (0.0185 \pm 0.0003)\,\mathrm{nm}$. The interpretation of this spectrum is analogous to the original laser spectrum of Figure 19. Also the same limitations due to limited resolution of the spectrum analyzer take place.

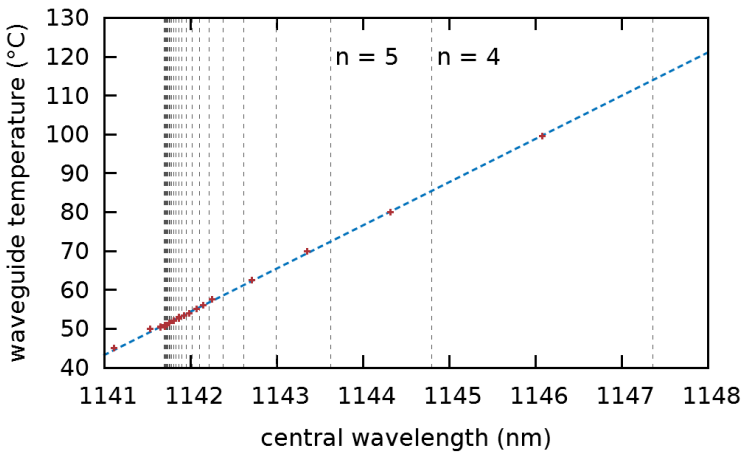

Figure 24: Ideal temperature for the quasi-phase match condition. The measruement data (red) are fitted with a linear function (blue) $T(\lambda) = 11.12\,°C\,nm^{-1} \cdot \lambda - 12\,650\,°C$. The gray vertical lines indicate the theoretical exciton states for the corresponding SHG.

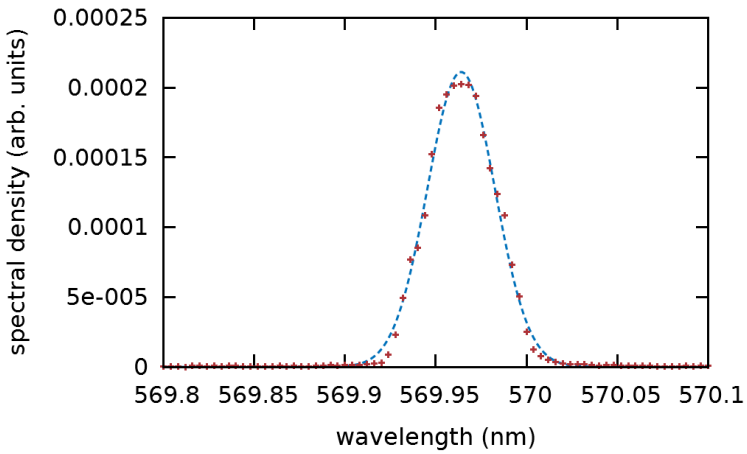

Figure 25: Spectrum of the SHG. The measurement data (red) are fitted with a Gaussian function (blue) $S(\lambda)$.

8 CUPROUS OXIDE

In this thesis the transmission spectrum of Cu_2O is investigated. An artificial crystal about 100 µm thick is used, whose temperature was held at about 1.9 K. Figure 26 shows the measured spectrum, where the excitons with the main quantum number $n = 4$ to $n = 9$ are clearly visible. This spectrum was taken by using the technique of amplitude modulation spectroscopy, which is described in Section 5.1.

8.1 CALIBRATION

The spectrum analyzer used in this experiment has a calibration error of about 0.3 nm around 632.8 nm. This error was detected by looking at the spectrum of a helium-neon laser, which has a well known central wavelength around 632.8 nm.

For the calibration the exciton absorption lines itself are used. As the reference the measured exciton energies of [3] are used (see Table 4 in Appendix A). The spectrum is calibrated at the exciton absorption line with the main quantum number $n = 6$, which has an energy of 2.169 48 eV.

Therefore the measured spectrum has to be shifted by −0.87 eV. This corresponds to a wavelength shift of 0.229 nm at 571.493 nm.

8.2 FIT OF ABSORPTION LINES

The absorption lines of the excitons with the main quantum numbers $n = 4$ to $n = 8$ are each fitted with an asymmetric Lorentzian function (see Equation 38). As the background a linear function is assumed individually for each absorption line. Consequently the fit function is given by the equation

$$\alpha_n(E) = C_n \frac{\frac{\Gamma_n}{2} + 2q_n \cdot (E - E_n)}{\left(\frac{\Gamma_n}{2}\right)^2 + (E - E_n)^2} + a_n \cdot (E - E_n) + b_n \tag{57}$$

with the six fit parameters C_n, Γ_n, E_n, q_n, a_n and b_n. The process is sketched in Figure 27.

The fit parameter C_n is proportional to the peak area (integral of the pure Lorentzian function), which is proportional to the oscillator strength. The variable Γ_n is the FWHM of the distribution and q_n describes the asymmetry. The variable E_n describes the energy of the exciton transition.

The parameter a_n and b_n determine the approximated background due to phonon assisted exciton absorptions into other exciton states.

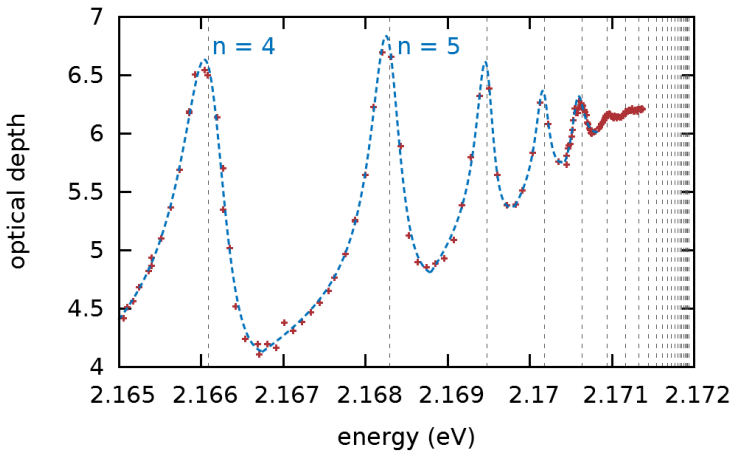

Figure 26: Spectrum of the yellow exciton series of an artificial Cu_2O crystal at 1.9 K up to the main quantum number $n = 9$. The first five absorption peaks are fitted with an asymmetric Lorentzian functions (blue). The vertical gray lines indicate the reference exciton states up to $n = 25$ [3].

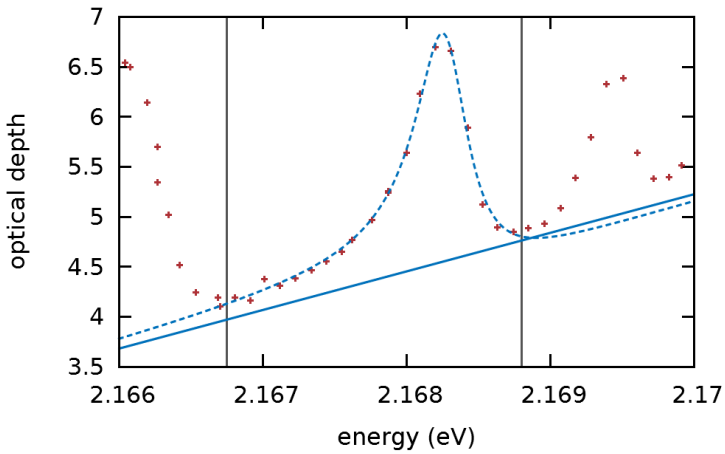

Figure 27: Fit of a single absorption line ($n = 5$). The absorption line is fitted with an asymmetric Lorentzian function. The range within which the spectrum (red) is fitted is indicated by the two vertical black lines. As the background an individual linear function is assumed for each absorption line (blue curve), which is added to the Lorentzian profile (blue dotted line).

Table 1: Fit parameters E_n, Γ_n and C_n of the absorption lines.

n	E_n (eV)	Γ_n (μeV)	C_n (10^{-3})
4	$2.166\,139 \pm 0.000\,005$	634 ± 10	0.699 ± 0.009
5	$2.168\,284 \pm 0.000\,005$	438 ± 9	0.485 ± 0.007
6	$2.169\,481 \pm 0.000\,005$	255 ± 11	0.177 ± 0.005
7	$2.170\,166\,6 \pm 0.000\,000\,7$	200 ± 2	0.0835 ± 0.0005
8	$2.170\,579 \pm 0.000\,003$	185 ± 5	0.0511 ± 0.0009

Table 2: Fit parameters q_n, a_n and b_n of the absorption lines.

n	q_n	a_n	b_n (eV^{-1})
4	-0.390 ± 0.010	4.15 ± 0.02	330 ± 30
5	-0.187 ± 0.009	4.57 ± 0.02	390 ± 20
6	-0.242 ± 0.018	4.94 ± 0.02	750 ± 60
7	-0.138 ± 0.003	5.288 ± 0.002	778 ± 6
8	0.111 ± 0.013	5.789 ± 0.006	580 ± 60

In Table 1 and Table 2 the six fit parameters for all five exciton absorption lines are listed.

8.3 ANALYSIS

The fit parameters of the exciton absorption parameters correspond to some physical properties of the excitons and the Cu_2O crystal.

8.3.1 *Linewidth and Oscillator Strength*

The parameters Γ_n correspond to the linewidth of the absorption lines and therefore determine with Equation 35 lower limits for the lifetimes of the excitons. The calculated values are listed in Table 3.

Figure 28b shows the linewidths as a function of n. The measurement data is fitted with a inverse cubic function (inspired by [3])

$$\Gamma(n) = \frac{a}{n^3} \tag{58}$$

with the fit parameter $a = (455 \pm 45)\,meV$. As it can be seen in Figure 28b the fit function does not coincide optimally with the measurement data.

The linewidths for the higher main quantum numbers are broader than expected. Possible reasons for this behavior could be crystallographic defects, whose influence increases with the main quantum number due to the exciton's larger spatial extension.

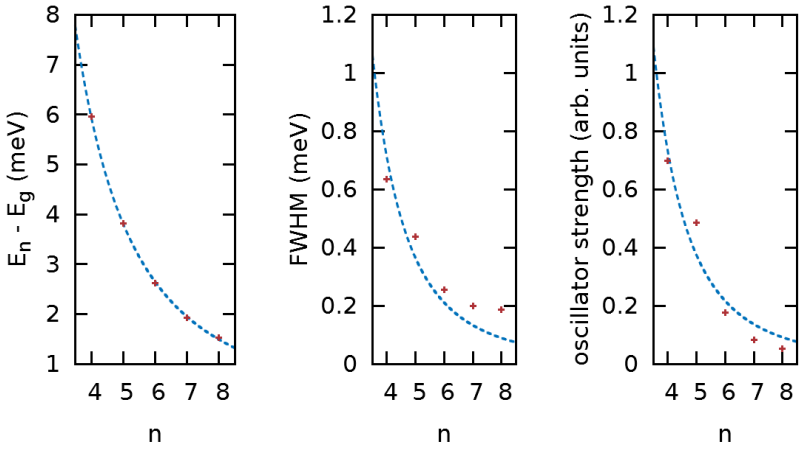

(a) Binding energy. (b) Linewidth. (c) Oscillator strength.

Figure 28: Analysis of exciton absorption linewidth parameters. a) The determined binding energies (red) fit perfectly to the estimated n^{-2} dependency. b) The linewidths (red) of the absorption lines should have an n^{-3} dependency (blue). c) The peak area (oscillator strength) (red) should decrease with an n^{-3} dependency (blue).

The same can be done with the oscillator strength, which is represented by the parameter C_n. In Figure 28c the parameters C_n are plotted over n (multiplied by 10^3) and are also fitted with a inverse cubic function

$$C(n) = \frac{b}{n^3} \ , \tag{59}$$

where the fit parameter is determined to $b = 0.046 \pm 0.004$. The good approximation shows, that the oscillator strength has an n^{-3} dependence, which confirms the theoretical expectations [3].

8.3.2 *Binding Energy*

The energy levels E_n in Table 1 can be fitted with the equation (see Equation 5)

$$E_n = E_g - \frac{E_R}{n^2} \ , \tag{60}$$

where $E_g = (2.172\,10 \pm 0.000\,03)\ eV$ is the band gap energy and $E_R = (95.27 \pm 0.09)\ meV$ the Rydberg energy. The implementation of the concept of quantum defects (see Equation 12) does not improve the fit. This effect may only be relevant for high main quantum numbers [3]. The band gap energy matches well with the reference of 2.172 08 eV, while the Rydberg energy differs about 3 meV compared to the reference of 92 meV [3] or 98.1 meV [10].

Table 3: Average radius and lifetime of the measured excitons

n	$\langle r_n \rangle$ (Å)	τ_n (ps)
4	269	1.04
5	427	1.50
6	620	2.58
7	848	3.29
8	1110	3.56

Figure 28a shows the binding energy ($E_n - E_g$) as a function of the main quantum number n. The exact n^{-2} dependence is clearly visible as described by the theoretical model. The description of excitons as hydrogen equivalent particles fits very well.

With the Rydberg energy E_R the Bohr radius (see Equation 7)

$$a_B = \frac{e^2}{8E_R \pi \epsilon_r \epsilon_0} = 11.7\,\text{Å} \ , \tag{61}$$

with the relative permittivity $\epsilon_r = 6.46$ [11]. For the exciton with the main quantum number $n = 9$ this corresponds to an average radius of (see Equation 13)

$$\langle r_n \rangle = \frac{1}{2} a_B \left(3n^2 - l \cdot (l+1)\right) = 1410\,\text{Å} \ , \tag{62}$$

which is about the fourth of the visible light's wavelength. The values of the other excitons are listed in Table 3.

With Equation 7 also the reduced mass

$$\mu^* = \frac{32\pi^2 \hbar^2 \epsilon_r^2 \epsilon_0^2 E_R}{e^4} = 0.29 \cdot m_e \tag{63}$$

of the excitons can be calculated, where $m_e = 9.109 \cdot 10^{-31}$ kg is the electron rest mass.

8.4 LIMITATIONS

The setup used to measure the transmission spectrum in Section 5.1 has some limitations:

The waveguide's phase match condition prevents the investigation of the excitons with the main quantum numbers $n = 3$ or $n = 2$, because therefore temperatures above 100 °C are necessary, which eventually destroy the waveguide directly or indirectly by damaging the mounting parts. However for the investigation of Rydberg excitons only high main quantum numbers are of interest.

For very highly excited excitons ($n > 15$) the resolution of the spectrum analyzer limits the direct measurement of the spectrum. However mode-hop free tuning can eventually exceed this limitation.

The resolution of the transmission is limited by the SNR. Due to the thickness of the sample, the transmission is very low in general. A very low laser power (about 300 µW) and a poorly optimized cryostat lead to very low power levels at the detector. For excitons with a main quantum number higher than $n = 9$ the signal drops drastically and therefore decreases the SNR. A possible explanation for his behavior could be phonon-assisted absorption (see Section 1.1.4) into other exciton states (including the 1s-state) [12]. This limitation could become less important by reducing the sample temperature.

The whole setup is also not damped against vibration, although the vacuum pumps used are powerful sources of vibration. Through the amplitude modulation spectroscopy the SNR of the signal could be increased drastically but not sufficient for the highly excited excitons.

CONCLUSION

Highly excited excitons are a relative new field of research. The setup described in this thesis is suitable for the investigation of Rydberg excitons in the semiconductor Cu_2O even if there are some limitations. It was possible to detect excitons with a main quantum number up to $n = 9$.

The theoretical properties of the laser and the waveguide could be confirmed and understood. The problems regarding mode hops could be explained.

Moreover some properties of the excitons and the material themselves could be investigated. For the band gap of Cu_2O an energy of $(2.172\,10 \pm 0.000\,03)$ eV was determined. The excitons' binding energies fit the theoretical model of the hydrogen- equivalent description with high precision. The corresponding Rydberg energy has a value of (95.27 ± 0.09) meV.

Different implementations of modulation spectroscopy were discussed and tested. With this setup only the amplitude modulation spectroscopy led to good results. It was superior regarding the signal-to-noise ratio compared to normal transmission spectroscopy.

For this experiment an artificial grown cuprous oxide crystal was used. Usually natural Cu_2O crystals are superior concerning crystal quality. In this thesis it could be shown at first that also artificial grown Cu_2O crystals show clear exciton absorptions up to the main quantum number $n = 9$. This overcomes a lot of limitations that could occur due to the restriction on natural crystals, regarding possible applications.

OUTLOOK

With this setup it is possible to investigate Rydberg excitons up to the main quantum number $n = 9$ in an artificial Cu_2O crystal. For further experiments some optimizations have to be applied to the setup:

First a reduction of the sample thickness down to values of 30 µm could be a great enhancement compared to the present 100 µm. A thinner crystal has a much higher transmission and so simplifies the detection and improves the SNR.

In the same way a cryostat optimized for the transmission of visible light around 571 nm can reduce the absorption, reflection and scattering of the cryostat. This leads to a higher and more stable intensity on the sample, which also reduces the SNR of the signal. An optimized cryostat with potentially smaller windows furthermore allows lower temperatures due to the reduced thermal radiation.

Also a spectrum analyzer or a wavemeter with a higher accuracy can resolve excitons with greater main quantum numbers.

Last but not least the optical setup can be improved. If the distance between the diode laser and the waveguide could be decreased drastically, this could reduce the effort of optimizing the coupling into the waveguide and therefore accelerate the measurement speed. With a spectrum analyzer or wavemeter with a digital output automation (e.g. the control of the waveguide temperature) is possible.

With these optimizations also further experiments with the crystal itself are possible. It could be interesting to investigate the influence of magnetic or electric fields on the exciton absorptions. Also intensity dependent measurements could be of interest. Moreover the comparison of artificial and natural crystals can be investigated.

Part IV

APPENDIX

A

EXCITON ENERGIES OF THE YELLOW SERIES

Table 4: High-precision exciton energies of he yellow series in Cu_2O. These exciton energies are published in [3] (supplementary Table S1).

n	E_n (eV)
2	2.1484
3	2.161 35
4	2.166 09
5	2.168 29
6	2.169 48
7	2.170 182
8	2.170 635
9	2.170 944
10	2.171 163
11	2.171 324
12	2.171 446
13	2.171 541
14	2.171 615 9
15	2.171 675 8
16	2.171 724 8
17	2.171 765 3
18	2.171 798 9
19	2.171 827
20	2.171 851 5
21	2.171 872 4
22	2.171 890 6
23	2.171 906 8
24	2.171 920 2
25	2.171 933 5

BIBLIOGRAPHY

[1] T. C. Chiang and F. J. Himpsel, "2.1.15 GaAs," in "Subvolume A," , vol. 23a of *Landolt-Börnstein - Group III Condensed Matter*, A. Goldmann and E.-E. Koch, eds. (Springer-Verlag, Berlin/Heidelberg, 1989), pp. 47–55.

[2] S. Hunklinger, *Festkörperphysik*, De Gruyter Studium (De Gruyter, München, 2014), 4th ed.

[3] T. Kazimierczuk, D. Fröhlich, S. Scheel, H. Stolz, and M. Bayer, "Giant Rydberg excitons in the copper oxide Cu2O," Nature **514**, 343–347 (2014).

[4] T. F. Gallagher, "Rydberg atoms," Reports on Progress in Physics **51** (1988).

[5] W. Demtröder, *Experimentalphysik 2: Elektrizität und Optik*, Springer-Lehrbuch (Springer, Berlin, 2013), 6th ed.

[6] R. Paschotta, "Quasi-phase matching," https://www.rp-photonics.com/quasi_phase_matching.html.

[7] Toptica Photonics, "Tunable laser diodes," http://www.toptica.com/fileadmin/user_upload/products/Diode_Lasers/Research_Grade/Tunable_Diode_Lasers/toptica_BR_SC_TDL.pdf.

[8] Stanford Research Systems, "About lock-in amplifiers: Application note #3," http://www.thinksrs.com/downloads/PDFs/ApplicationNotes/AboutLIAs.pdf.

[9] Toptica Photonics, "Dl pro: Tunable diode laser," http://www.toptica.com/products/research_grade_diode_lasers/tunable_diode_lasers/the_ultimate_tunable_diode_laser_dl_pro.html.

[10] H. Matsumoto, K. Saito, M. Hasuo, S. Kono, and N. Nagasawa, "Revived interest on yellow-exciton series in Cu2O: An experimental aspect," Solid State Communications **97**, 125–129 (1996).

[11] "Cuprous oxide (Cu2O) dielectric constant," in "Non-Tetrahedrally Bonded Elements and Binary Compounds I," , vol. 41C of *Landolt-Börnstein - Group III Condensed Matter*, O. Madelung, U. Rössler, and M. Schulz, eds. (Springer-Verlag, Berlin/Heidelberg, 1998), pp. 1–2.

[12] A. Jolk, "Spektroskopische Untersuchungen an Cu2O," Diplomarbeit, Universität Karlsruhe, Karlsruhe (1997).

DECLARATION

I hereby declare that this thesis entitled 'Modulation Spectroscopy of Rydberg Excitons' has been carried out at the 4th Physics Institute, University of Stuttgart, Germany under guidance of Prof. Dr. Harald Gießen and Tobias Steinle.

Furthermore I certify that this thesis is my original work and has not been submitted in part or full by me for any degree or diploma at any other university. The material obtained from other sources has been indicated clearly.

Stuttgart, November 2015

Sven Bodenstedt